JOURNAL OF Materials CHEMISTRY

# The effects of mechanical activation in synthesizing ultrafine barium ferrite powders from co-precipitated precursors

**X. Liu,[a] J. Wang,*[a] J. Ding,[a] M. S. Chen[b] and Z. X. Shen[b]**

[a]*Department of Materials Science, Faculty of Science, National University of Singapore, Singapore 119260*
[b]*Department of Physics, Faculty of Science, National University of Singapore, Singapore 119260*

***Received 3rd December 1999, Accepted 28th April 2000***
***Published on the Web 8th June 2000***

Well dispersed and fine barium ferrite ($BaFe_{12}O_{19}$) powders have been successfully prepared by mechanically activating co-precipitated precursors, followed by calcination at 700 and 800 °C. When mechanically activated in a sodium chloride matrix for 20 hours, nanocrystallites of $BaFe_{12}O_{19}$, $\alpha$-$Fe_2O_3$ and a spinel ($\gamma$-$Fe_2O_3$) phase of $<10$ nm in size were triggered in the co-precipitated precursor. Single phase barium ferrite platelets 50–100 nm in size were developed upon subsequent calcination at 800 °C for 1 hour. The resulting barium ferrite powder exhibits an intrinsic coercivity ($_iH_c$) of 436.7 kA $m^{-1}$ and a saturation magnetization ($M_s$) of 67.8 A $m^2$ $kg^{-1}$. These magnetic properties compare favorably with those of the materials derived from conventional calcination of the co-precipitated precursor without prior mechanical activation, which led to very poor powder characteristics.

## Introduction

Barium ferrite ($BaFe_{12}O_{19}$) has been widely studied as a permanent magnet and more recently for high density magnetic recording.[1,2] As a recording medium, it is chemically stable and resistant to corrosion. It also offers the possibility of setting the coercivity at a desirable value through appropriate dopants (*e.g.* Co, Ti or Ni, Zn).[3] For ideal performance during magnetic recording, the barium ferrite particles are required to be single domain, chemically homogeneous, and exhibit a high saturation magnetization, large coercivity, narrow size distribution and good dispersibility.[4]

Traditional ceramic processing for synthesizing barium ferrite powders involves mixing and subsequently firing a powder mixture of iron oxide and barium carbonate at a high enough temperature (*ca.* 1200 °C). It has the advantages of low production cost and high production yield, but the detrimental consequences, such as low compositional homogeneity, strong particle aggregation and wide particle size distribution, make it unsuitable for synthesizing materials designed for use in recording media. Various alternative processes have therefore been developed to prepare ultrafine barium ferrite powders with the desired particle characteristics. They are specifically aimed at applications for high density perpendicular recording media. These include coprecipitation,[5,6] glass crystallization,[7,8] organometallic precursor methods,[9] sol–gel techniques,[10] and hydrothermal reactions.[11,12] One of their common aims is to achieve a high mixing homogeneity in the precursor state so that the subsequent reaction for forming barium ferrite can occur at relatively low temperatures. Thus the unwanted particle coarsening and aggregation can be minimized or avoided.

Mechanical alloying was devised and employed to prepare a number of metal and alloy powders.[13–16] It has recently been adopted to synthesize ferrite-based magnetic materials and ceramics.[17–20] In fact, many of the reactions and phase transformations, including decomposition, crystallization and dehydration, which are traditionally realized through solid state reaction by calcination at an elevated temperature, can be triggered by mechanical activation at room temperature.[21,22] Unfortunately, the mechanochemically derived ferrite and ceramic powders often exhibit poor particle characteristics, represented by a wide particle size distribution and irregular particle morphology, and a degree of particle aggregation. This is a consequence of the fact that the powder particles are subjected to repeated impacts and local compaction in an uncontrolled manner. On the other hand, little success has been achieved in the case of ultrafine $BaFe_{12}O_{19}$ *via* mechanical activation routes, although several attempts have been made. Ding *et al.*[23] tried to synthesize $BaFe_{12}O_{19}$ platelets 20–100 nm in diameter and 10–20 nm in thickness *via* mechanochemical reaction between $BaCl_2$ and $FeCl_3$ in NaOH and calcination at 800 °C. Osami Abe *et al.*[24] reported a solid-state reaction route for $BaFe_{12}O_{19}$ and the resulting powder consisted of particle agglomerates *ca.* 1 μm in size. However, a nanocrystalline $BaFe_{12}O_{19}$ phase was not realized by mechanical activation in these studies. We report in this paper the occurrence of ultrafine crystallites of $BaFe_{12}O_{19}$ triggered by mechanical activation of a co-precipitated precursor. By a close comparison with the conventional coprecipitation followed by calcination without prior mechanical activation, it is demonstrated that the mechanical activation in sodium chloride is effective in leading to ultrafine $BaFe_{12}O_{19}$ particles with excellent particle and magnetic properties.

## Experimental

The starting materials were commercially available barium nitrate and ferric nitrate of reagent grade [$Ba(NO_3)_2$ and $Fe(NO_3)_3{\cdot}9H_2O$, purity >99%, Fisher Scientific], ammonium hydroxide solution (28.0–30.0% $NH_3$, Ajax Chemicals, Australia) and sodium chloride (purity >99.5%, 0.3–0.5 mm particle size and cubic morphology, Merck, Germany). $Ba(NO_3)_2$ and $Fe(NO_3)_3{\cdot}9H_2O$ were first dissolved in deionized water to prepare an aqueous solution containing $Ba^{2+}$ and $Fe^{3+}$ in a molar ratio of 1 : 7. The solution was then titrated into an ammonia solution of pH ~ 10 to co-precipitate Ba–Fe hydroxides. The hydroxide precipitates were retrieved by filtration, washed using deionized water and then freeze-dried. The resulting hydroxide precursor powder was divided into two batches. The first batch was subjected to mechanical

activation in sodium chloride for up to 20 hours, where the sodium chloride to precursor weight ratio was controlled at 4 : 1. The sodium chloride–precursor mixture was then sealed in a stainless vial 5.7 cm in diameter and 10.2 cm in length together with stainless steel balls 10 mm in diameter. The ball to powder weight ratio was controlled at *ca.* 12 : 1. Mechanical activation was carried out in a Spex 8000 high energy shaker mill. The activated powder was then calcined at 700 and 800 °C (1 hour at each temperature), followed by washing using deionized water to remove sodium chloride. The second batch of hydroxide precursor powder was directly calcined at 700 and 800 °C (1 hour at each temperature), without any mechanical activation.

Differential thermal analysis (DTA) and thermogravimetric analysis (TGA) were performed on the mechanically activated and calcined powders using a DuPont 2950 thermal analyzer in air at a heating rate of 10 °C $min^{-1}$ from room temperature to 900 °C. The phases present in each were analyzed using a powder X-ray diffractometer (Cu-K$\alpha$, Phillips PW1729 X-ray Diffractometer) operated at 30 KV and 20 mA. They were also analyzed using a Raman spectrometer (spex 1702/04 Raman spectrometer with an Olympus microscope attachment). Transmission electron microscopes (TEM, JEOL-100CX and Philips CM300 FEG) were employed to examine their particle characteristics. Their magnetic properties, such as intrinsic coercivity ($_iH_c$) and saturation magnetization ($M_s$), were measured using a vibrating sample magnetometer (VSM, 9T, Oxford Instruments).

## Results and discussion

Fig. 1 shows the DTA traces of the as-dried hydroxide precursor and the mechanically activated sample after removal of sodium chloride by washing using deionized water. Three endothermal/exothermal peaks were observed for the as-dried precursor. The broadened endothermal peak located below 200 °C is attributed to the elimination of absorbed water and moisture of the hydroxide precursor. The broadened exothermal peak over the temperature range 200–300 °C is due to the decomposition of hydroxides and the formation of crystalline oxides. This is followed by an exothermal peak at *ca.* 730 °C, due to the formation of crystalline barium ferrite. Similarly, the mechanically activated powder exhibits a broadened endothermal peak over the temperature range 80–150 °C due to the elimination of residual water content and moisture. However, the intensity of the exothermal reaction over the temperature range 700–800 °C, which is attributed to the formation of barium ferrite, is minimized. This suggests that the reaction responsible for the formation of barium ferrite is largely completed by the mechanical activation. This is supported by the occurrence of a broadened exothermal peak in the temperature range 500–600 °C, as will be discussed later,

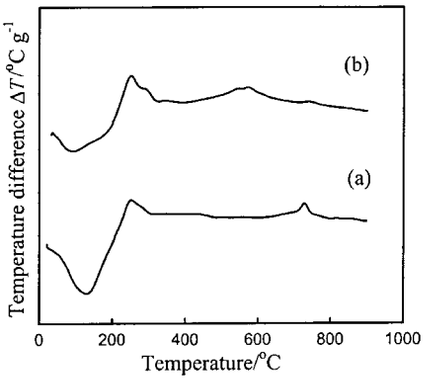


**Fig. 1** The DTA curves of (a) the coprecipitated hydroxide precursor, and (b) the mechanically activated powder precursor.

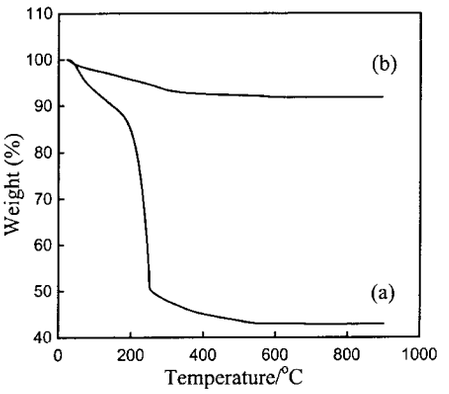


**Fig. 2** TGA curves of (a) the coprecipitated hydroxide precursor, and (b) the mechanically activated powder precursor.

which is attributed to the increase in crystallinity of barium ferrite and the transitional $\alpha$-$Fe_2O_3$ and $\gamma$-$Fe_2O_3$ phases.

Fig. 2 shows the TGA curves for the as-dried hydroxide precursor and the precursor powder mechanically activated for 20 hours in sodium chloride. The as-dried hydroxide precursor exhibits two apparent steps of weight loss, *i.e.* a slow and steady one from room temperature to *ca.* 180 °C and a fall in specimen weight from *ca.* 180 to 270 °C. Little further weight loss is observed at temperatures above 500 °C, indicating the completion of any reactions involving a weight change. As discussed earlier, the slow and steady weight loss from room temperature to *ca.* 180 °C is due to the elimination of residual water and moisture. The sharp fall in specimen weight over the temperature range 180–270 °C is related to the decomposition of hydroxides into oxides. The total weigh loss of the as-dried hydroxide precursor is about 56%. In contrast, the mechanically activated powder exhibits a much lower total weight loss (6–7%) at temperatures below 500 °C. This suggests that the hydroxide to oxide conversion is largely completed by the mechanical activation.

Fig. 3 shows the XRD patterns for the as-dried hydroxide precursor, as well as for the material subjected to 20 hours of mechanical activation without calcination, after calcination at 700 °C (1 hour), and after subsequent calcination at 800 °C (1 hour). As expected, the co-precipitated hydroxide precursor exhibits a highly amorphous nature, as suggested by the broadened peak over the $2\theta$ range 30–38°. Its amorphous nature was also supported by the diffused rings in the selected area diffraction pattern *via* TEM. After 20 hours of mechanical activation, nanocrystallites of $\alpha$-$Fe_2O_3$, $\gamma$-$Fe_2O_3$ and

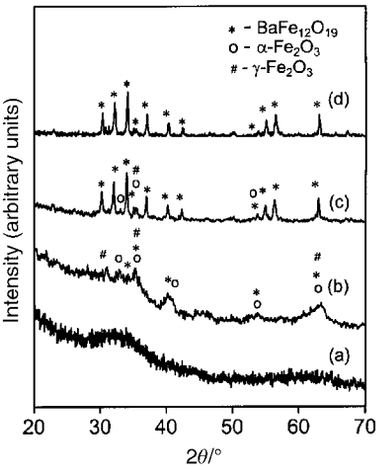


**Fig. 3** XRD patterns of (a) coprecipitated hydroxide precursor, (b) mechanically activated powder precursor, (c) the powder calcined at 700 °C for 1 hour after mechanical activation, and (d) the powder subsequently calcined at 800 °C for 1 hour after mechanical activation.

$BaFe_{12}O_{19}$ were observed as indicated by the broadened peaks at $2\theta$ values of *ca.* 30.5, 32.2, 33.2, 34.1, 35.6, 40.3 and 63.1°. As expected, calcination at 700 °C for 1 hour significantly reduced the amounts of the $\alpha$-$Fe_2O_3$ and $\gamma$-$Fe_2O_3$ phases and, at the same time, $BaFe_{12}O_{19}$ of improved crystallinity was established as the principal crystalline phase. The crystallinity of $BaFe_{12}O_{19}$ was further enhanced when the calcination temperature was raised to 800 °C, while the transitional $\alpha$-$Fe_2O_3$ and $\gamma$-$Fe_2O_3$ phases were largely eliminated. Calcination of the precipitated hydroxide precursor at 700 °C for 1 hour without prior mechanical activation led to a mixture of $\alpha$-$Fe_2O_3$ and $BaFe_{12}O_{19}$. A predominant $BaFe_{12}O_{19}$ phase resulted when the unactivated hydroxide precursor was calcined at 800 °C for 1 hour.

To further support what is shown by XRD phase analysis, Fig. 4 shows the Raman spectra for the as-dried hydroxide precursor, as well as for the material subjected to 20 hours of mechanical activation without calcination, after calcination at 700 °C (1 hour), and after subsequent calcination at 800 °C (1 hour). The absence of apparent sharp peaks in the Raman spectrum supports the highly amorphous nature of the as-dried hydroxide precursor. Upon mechanical activation for 20 hours, strong and broadened peaks are observed at 336, 411, 527, 616 and 684 $cm^{-1}$, indicating the formation of a barium ferrite phase.[25] At the same time, the peaks formed at *ca.* 244 and 293 $cm^{-1}$ are attributed to a nanocrystalline $\alpha$-$Fe_2O_3$ phase.[26] The small humps at *ca.* 350, 500 and 700 $cm^{-1}$ also indicate the presence of a minor amount of $\gamma$-$Fe_2O_3$. This therefore shows that nanocrystallites of $BaFe_{12}O_{19}$, $\alpha$-$Fe_2O_3$ and a minor amount of $\gamma$-$Fe_2O_3$ were triggered by 20 hours of mechanical activation. Upon calcination at 700 and 800 °C for 1 hour at each temperature, the transitional $\alpha$-$Fe_2O_3$ and $\gamma$-$Fe_2O_3$ phases were largely eliminated and $BaFe_{12}O_{19}$ was realized as the predominant crystalline phase.

The bright field TEM micrographs and selected area diffraction (SAD) patterns taken for the as-dried precursor, the material subjected to 20 hours of mechanical activation, and that subjected to further calcination at 800 °C, are shown in Fig. 5(a–c), respectively. The hydroxide precursor consists of particle agglomerates of irregular morphology and size. The very diffused SAD pattern confirms its amorphous nature. Upon mechanical activation in NaCl for 20 hours, there occurs a refinement in the size of the hydroxide agglomerates into the range 50–100 nm. Furthermore, discrete particles of $<10$ nm were clearly visible in these agglomerates. Their nanocrystalline nature is shown by the sharpened spotty ring in the selected area diffraction pattern. This was confirmed by a study using high resolution TEM, which reveals the occurrence of nanocrystallites in an amorphous matrix. Fig. 6 is an example of such a high resolution TEM observation, where the nanodomains of $BaFe_{12}O_{19}$, $\alpha$-$Fe_2O_3$ and $\gamma$-$Fe_2O_3$ can be located. As illustrated in Fig. 5(c), there is a dramatic change in particle morphology when the activated powder was further calcined at 800 °C for 1 hour. The resulting barium ferrite powder consists of platelets of 50 to 100 nm, which are well dispersed. Its well established crystalline nature is supported by the multiple spot rings in its diffraction pattern. Fig. 7 further shows the particle size distribution in this powder calculated on the basis of TEM observations, with an average particle size of $67 \pm 23$ nm. For comparison, Fig. 8 is a bright field TEM micrograph for the $BaFe_{12}O_{19}$ derived from co-precipitated precursor *via* calcination at 800 °C without prior mechanical activation. The barium ferrite powder consists of particles 80–200 nm in size, which are highly irregular in morphology and do not exhibit a well established hexagonal morphology.

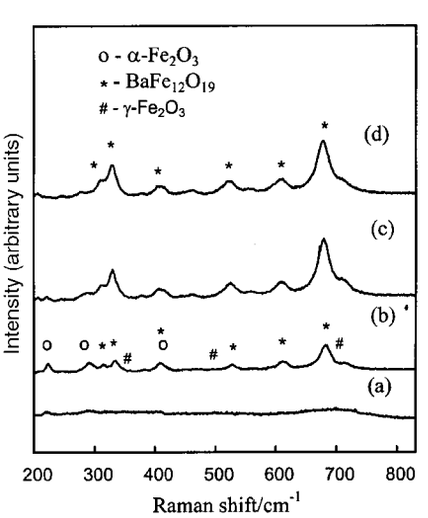


**Fig. 4** Raman spectra of (a) the as-dried hydroxide precursor, (b) the mechanically activated powder precursor, (c) the powder calcined at 700 °C for 1 hour after mechanical activation; and (d) the powder subsequently calcined at 800 °C for 1 hour after mechanical activation.

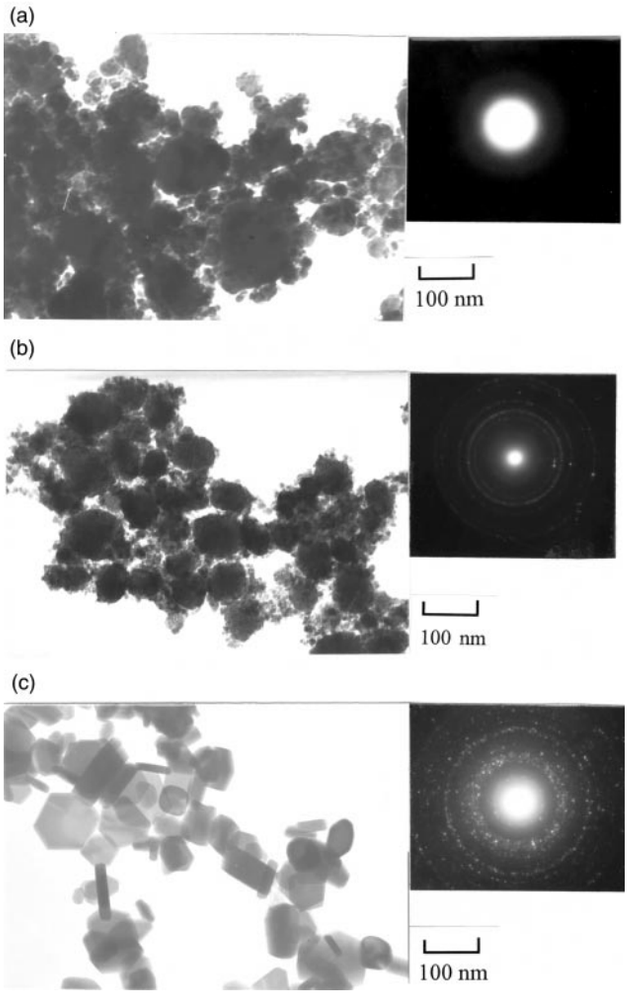


**Fig. 5** Bright field TEM micrographs and selected area diffraction patterns for (a) the hydroxide precursor, (b) the mechanically activated powder, and (c) the mechanically activated powder calcined at 800 °C for 1 hour.

The magnetic properties of the materials subjected to various treatments were measured at room temperature (291 K). Fig. 9 shows the hysteresis loops for the powder subjected to 20 hours of mechanical activation and those subsequently calcined at 700 and 800 °C. As discussed earlier, 20 hours of mechanical activation led to the occurrence of nanocrystallites of $BaFe_{12}O_{19}$ and $\alpha$-$Fe_2O_3$, together with a minor amount of $\gamma$-$Fe_2O_3$. However, their magnetic properties were not observed by the VSM measurement. This can easily be accounted for by

the nanocrystalline structure and poor crystallinity of $BaFe_{12}O_{19}$. As has been observed using HRTEM, the activation-triggered $BaFe_{12}O_{19}$, $\alpha$-$Fe_2O_3$ and $\gamma$-$Fe_2O_3$ crystallites are less than 10 nm in size, and are dispersed in an amorphous matrix. At such a refined crystallite size, a ferrimagnetic material exhibits superparamagnetic behavior.[27] Furthermore, the magnetic behavior of $BaFe_{12}O_{19}$ is strongly dependent on its crystallinity, *e.g.* the angle of the Fe–O–Fe bond.[3,28] The 20 hours of mechanical activation triggered the occurrence of $BaFe_{12}O_{19}$ nanocrystallites $<10$ nm in size together with nanocrystalline $\alpha$-$Fe_2O_3$ and $\gamma$-$Fe_2O_3$ phases, the poor crystallinity of which has been indicated by the much broadened XRD and Raman spectra. As discussed earlier, calcination at 700 °C for 1 hour resulted in the $\alpha$-$Fe_2O_3$ and $\gamma$-$Fe_2O_3$ to $BaFe_{12}O_{19}$ conversion and the crystallinity of $BaFe_{12}O_{19}$ was much enhanced. Accordingly, the material exhibits a well defined hysteresis loop, characterized by $M_s = 45.8$ A m$^2$ kg$^{-1}$ and $_iH_c = 416.8$ kA m$^{-1}$. Calcination at 800 °C further enhances the saturation magnetization to $M_s = 67.8$ A m$^2$ kg$^{-1}$ and intrinsic coercivity to $_iH_c = 436.7$ kA m$^{-1}$, due to the further improvement in phase purity and crystallinity of the $BaFe_{12}O_{19}$ phase. In contrast, the materials derived from calcination without prior mechanical activation exhibited much poorer magnetic properties. For example, the barium ferrite powder calcined at 700 °C for 1 hour without prior mechanical activation demonstrated a saturation magnetization of $M_s = 44.2$ A m$^2$ kg$^{-1}$ and an intrinsic coercivity of $_iH_c = 306.2$ kA m$^{-1}$. Its saturation magnetization was raised to $M_s = 64.7$ A m$^2$ kg$^{-1}$ upon calcination at 800 °C for 1 hour. However, its intrinsic coercivity ($_iH_c = 353.2$ kA m$^{-1}$) was much lower than that of the barium ferrite powder ($_iH_c = 436.7$ kA m$^{-1}$) derived from mechanical activation. This is apparently due to the much coarsened particle size and poor powder characteristics, as discussed earlier. Coarsening in particle size can lead to a switch from a single domain structure to a multi-domain one, which results in a decrease in intrinsic coercivity.[29]

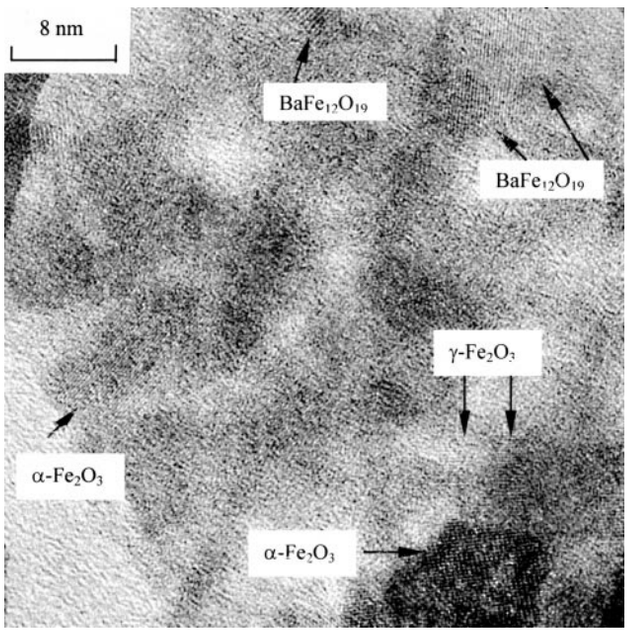


**Fig. 6** HRTEM micrograph for the mechanically activated powder precursor.

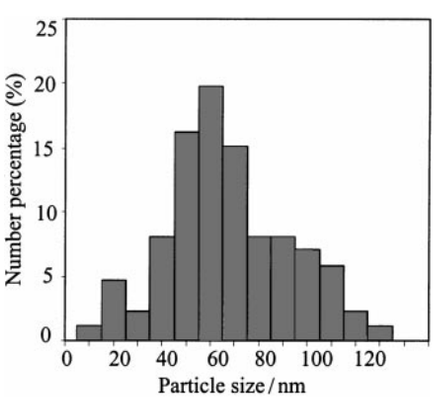


**Fig. 7** Particle size distribution of the powder prepared by mechanical activation for 20 hours followed by calcination at 800 °C for 1 hour.

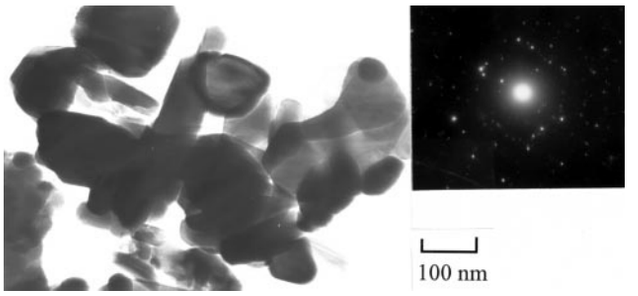


**Fig. 8** Bright field TEM micrograph and selected area diffraction pattern for the hydroxide precursor calcined at 800 °C for 1 hour without prior mechanical activation.

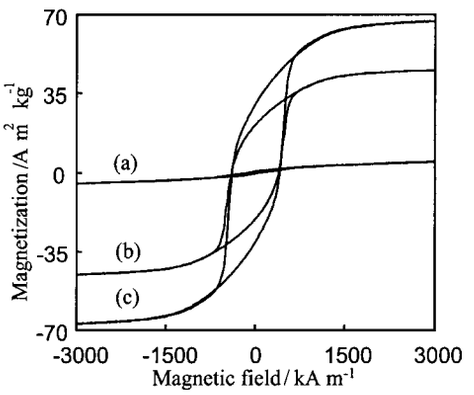


**Fig. 9** Hysteresis loops of (a) the mechanically activated powder, (b) the mechanically activated powder calcined at 700 °C for 1 hour, and (c) the mechanically activated powder calcined at 800 °C for 1 hour.

## Conclusions

Mechanical activation of a coprecipitated barium ferrite hydroxide precursor in sodium chloride for 20 hours triggers the formation of nanocrystallites of $BaFe_{12}O_{19}$, $\alpha$-$Fe_2O_3$ and $\gamma$-$Fe_2O_3$. The resulting material is largely paramagnetic due to the much refined crystallite size ($<10$ nm) and poor crystallinity of these phases. Subsequent calcination at 800 °C completes the $\alpha$-$Fe_2O_3$ and $\gamma$-$Fe_2O_3$ to $BaFe_{12}O_{19}$ conversion and leads to the formation of hexagonal $BaFe_{12}O_{19}$ platelets, which are 50–100 nm in size. The resulting material exhibits an intrinsic coercivity ($_iH_c$) of 436.7 kA m$^{-1}$ and a saturation magnetization ($M_s$) of 67.8 A m$^2$ kg$^{-1}$. These magnetic properties compare favorably with those of the material derived from conventional calcination of the precipitated precursor, which exhibits an extensive degree of particle coarsening and agglomeration and therefore a much degraded coercivity.

## References

1 D. Jiles, in *Introduction of magnetism and magnetic materials*, Chapman & Hall, London, 1991.
2 G. C. Hadjipanayis, in *Magnetic Hysteresis in Novel Magnetic*

*Materials*, NATO ASI series, Kluwer Academic Publishers, Netherlands, 1997, p. 769.
3 E. P. Wohlfarth, in *Ferromagnetic Materials*, North-Holland Publishing Company, Boston, MA, 1980, vol. 3.
4 G. C. Hadjipanayis and G. A. Prinz, in *Science and Technology of Nanostructured Magnetic Materials*, Plenum Press, New York, 1991, p. 497.
5 K. Haneda and H. Kojima, *J. Appl. Phys.*, 1973, **44**, 3760.
6 W. Roos, *J. Am. Ceram. Soc.*, 1980, **63**, 601.
7 O. Kabo. T. Ido and H. Yokoyama, *IEEE Trans. Magn.*, 1982, **MAG-18**, 1122.
8 H. Yokoyama, T. Maeda, T. Nomura, O. Kubo and T. Ido, *Ferrites: Proceeding of the Sixth International Conference on Ferrites (ICF 6)*, Tokyo and Kyoto, Japan, 1992, p. 1418.
9 F. Licci and T. Besagni, *IEEE Trans. Magn.*, 1984, **MAG-20**, 1639.
10 W. Zhong, W. Ding, N. Zhang, J. Hong, Q. Yan and Y. Du, *J. Magn. Magn. Mater.*, 1997, **168**, 196.
11 A. Ataie, M. R. Piramoon, I. R. Harris and C. B. Ponton, *J. Mater. Sci.*, 1995, **30**, 5600.
12 H. Kumazawa, Y. Maeda and E. Sada, *J. Mater. Sci. Lett.*, 1995, **14**, 68.
13 J. S. Benjamine, *Sci. Am.*, 1976, **234**, 40.
14 J. Ding, W. F. Miao, P. G. McCormick and R. Street, *Appl. Phys. Lett.*, 1995, **67**, 3804.
15 G. Cocco, G. Mulas and L. Schiffini, *Mater. Trans., JIM*, 1995, **36**, 150.
16 J. Ding, W. F. Miao, T. Tsuzuki, P. G. McCormick and R. Street, *J. Magn. Magn. Mater.*, 1996, **162**, 271.
17 W. A. Kaczmarek and B. W. Ninham, *IEEE Trans. Magn.*, 1994, **30**, 732.
18 P. Matteazzi and G. L. Caer, *Mater. Sci. Eng.*, 1991, **A149**, 135.
19 W. A. Kaczmarek and B. W. Ninham, *J. Phys. IV Fr.*, 1997, **7**, C1–47.
20 X. Liu, J. Ding and J. Wang, *J. Mater. Res.*, 1999, **14**(8), 3355.
21 V. V. Boldyrev, *Mater. Sci. Forum*, 1998, **227**, 269.
22 J. J. Gilman, *Science*, 1996, **274**, 65.
23 J. Ding, T. Tsuzuki and P. G. McCormick, *J. Magn. Magn. Mater.*, 1998, **931**, 177.
24 O. Abe and M. Narita, *Solid State Ionics*, 1997, **103**, 101.
25 J. Kresel, G. Lucazeau and H. Vincent, *J. Solid State Chem.*, 1998, **137**, 127.
26 D. L. A. De Farria, S. V. Silva and M. T. De Oliveira, *J. Raman Spectrosc.*, 1997, **28**, 873.
27 M. P. Morales, S. Veintemillas-Verdaguer and C. J. Serna, *J. Mater. Res.*, 1999, **14**(7), 3066.
28 A. Isalgue, A. Labarta, J. Tegada and X. Obradors, *Appl. Phys. A*, 1985, **38**, 3063.
29 R. Valenzuela, in *Magnetic Ceramics*, Cambridge University Press, Cambridge, 1994, p. 168.